Application of Stewart Platform as a Haptic Device for Teleoperation of a Mobile Robot

Duc-Vinh Le and CheolKeun Ha(✉)

School of Mechanical Engineering, University of Ulsan, Ulsan 44610, South Korea
cheolkeun@gmail.com

Abstract. In this study, a haptic device based on a Stewart Platform is developed by a dual-loop position-based admittance control. The admittance control is a common technology used in the haptic interface, which has two control loops. An outer loop transforms a force to the desired position and orientation, which is called an admittance model. An inner position loop based on a fault-tolerant control is used to ensure that the movement of the haptic device follows the reference trajectory resulting from the admittance model. The fault-tolerant control in this research is a combination of Nonsingular Fast Terminal Sliding mode control (NFTSMC) with an improved reaching law and an Extended State Observer (ESO), which is used to estimate and compensate for disturbances, uncertainties, and faults in the system. The ESO mentioned in this paper can reduce the peaking value and enhance the tolerance ability to measurement noise compared to the traditional ESO. Accordingly, this fault-tolerant control will enhance the performance of the system under uncertainties, disturbances, and make the haptic handle move smoothly even in the presence of faults in the system. Finally, the haptic device is applied for teleoperation of a mobile robot with force feedback that helps the operator prevent the robot from colliding obstacles and improve the task performance. The experimental results demonstrate the effectiveness of the proposed system.

Keywords: Haptic device · Admittance control · Teleoperation

1 Introduction

Teleoperation is a popular technology in robotics that enable humans to control robots remotely. These days, teleoperation is widely used to replace humans in many fields and hazardous environments such as surgery, deep water exploration, space exploration, and nuclear power plants.

Teleoperation includes a master device (haptic device), slave robot, and communication channels. The movement of the haptic device gives a position command sent to a slave robot. The feedback information such as interaction force and images are fed back to the master device. This is called bilateral teleoperation, which helps operators feel more realistic and enhance the user performance while doing a task. For example, considering a situation such as controlling a mobile robot, an operator moves the haptic handle

D.-S. Huang et al. (Eds.): ICIC 2022, LNAI 13395, pp. 80–92, 2022.
https://doi.org/10.1007/978-3-031-13832-4_7

to control the movement of the robot and the images showing the environment are sent to the operator. However, if the information are just images without depth information, it will be challenging for the user to prevent the robot from hitting obstacles. Therefore, depth information is required. When the robot approaches obstacles, it will give the force feedback rendered from the depth information to the operators through the haptic device. This feedback helps the operator notice that the robot is moving toward the obstacle. Hence, the development of a haptic device with feedback is necessary for the teleoperation system. There have been many investigations to advance haptic performance [1–4]. A haptic device based on an admittance control is a simple and efficient way that calculates a displacement corresponding to a force input. The relationship between the force and movement is imposed by a mass damper spring system. An admittance control often has two loops. The external loop as an admittance model is used to transform the force input into movements of a handle of the haptic device. The inner loop called position control is used to track the desired position given by the external loop. In the position control, the unknown uncertainty dynamics and disturbances cause a decrease in the system stability. In addition to unknown dynamics and disturbances, faults in the system seriously deteriorate the performance. In previous literature, the presence of faults was not considered in the haptic device, hence this research will investigate a fault-tolerant method for the inner position control of the haptic device. Fault-tolerant technologies for the tracking control have increasingly attracted many researchers over the years [5–8]. The remarkable feature of these technologies is to design a proper control law to tolerate some random faults in sensors, actuators, and other parts and guarantee whole system stability. In active fault-tolerant control (AFTC), the estimation module is used to observe the faults in the system and various methodologies have been studied in fault estimation [5–7]. An extended state observer (ESO) is an effective method and easy implementation for estimating uncertainties, disturbances, and faults. Nevertheless, the conventional ESO has several downsides such as the sensitivity to measurement noise and the peaking problem that may cause performance deterioration of the system. To eliminate these disadvantages of a traditional ESO, a new ESO [9] is proposed by Ran et al. for uncertain non-linear systems. The ESO in [9] illustrated the efficiency in decreasing the peaking value and augmenting the insensitivity to measurement noise. Therefore, thanks to those notable features, this paper will develop an AFTC for the inner loop control in the haptic device by combining a Nonsingular Fast Terminal Sliding Mode Control (NFTSMC) with an improved reaching law [10] and the ESO [9]. NFTSMC not only has the worthy attributes of robustness to uncertainties, disturbances, and low sensitivity to the changes in the system parameters, but also guarantees that the system quickly approaches the equilibrium point in a finite time. Besides, we proposed a new reaching law [10] to further enhance the performance of Sliding mode control. Consequently, the proposed controller inherits the advantages of NFTMSC with an improved reaching law [10] and ESO [9], and can considerably improve the efficiency and the stability of the system under the effect of uncertainties and faults. In this research, the actuator fault is considered and the fault-tolerant control is proposed to estimate and compensate for the bias and loss of effectiveness faults (gain faults) mentioned in [11].

Overall, our key idea is to build a haptic device based on the Stewart Platform using the admittance model and the proposed controller. The admittance model is used to

render the force impacting on the haptic handle measured by a force/torque sensor into the position and orientation of the haptic handle. The position and orientation are considered as the desired movements are fed to the proposed controller to control the haptic handle to follow the desired trajectory. The proposed controller will enhance the performance of the haptic device and make the haptic handle move smoothly under the existence of actuator faults. To assess the effectiveness of the haptic device using the suggested controller, the experiment result demonstrates a comparison of the proposed controller with the others. Finally, the haptic device will be applied for controlling a mobile robot and receiving force feedback from the robot to help the operator avoid collision and enhance task performance. The paper is organized as follows; the admittance model is described in Sect. 2. The active fault-tolerant control is designed in Sect. 3. The experiment result demonstrates the efficiency of the proposed controller and teleoperation of the mobile robot shown in Sect. 4. The conclusions are given in Sect. 5.

2 Admittance Model

The structure of the haptic device is shown in Fig. 1, which includes some main components such as a Stewart Platform, a force/torque sensor (F/T sensor) is mounted on the upper platform, and a handle is mounted on the F/T sensor. The admittance model regulates the relationship between the movement of the haptic handle and a contact force on the handle. The admittance equation for 1-DOF is described as

$$\frac{x_r(s)}{F(s)} = \frac{1}{M_i s^2 + B_i s + K_i} \tag{1}$$

where F is the force impacting on the handle, x_r represents the position of the haptic handle in task space, while M_i, B_i, and K_i describe Cartesian inertia, viscosity, and stiffness of the mechanical system, respectively. For a 6-DOF haptic device, x_r has six elements described as

$$\begin{bmatrix} t_x \\ t_y \\ t_z \\ \gamma \\ \beta \\ \alpha \end{bmatrix} = \frac{1}{M_i s^2 + B_i s + K_i} \begin{bmatrix} f_x \\ f_y \\ f_z \\ m_x \\ m_y \\ m_z \end{bmatrix} \tag{2}$$

where t_x, t_y, and t_z are the position of the haptic handle. α (Heave), β (Sway), and γ (Surge) are the orientation of the haptic handle. f_x, f_y, and f_z are the force measured by the force/torque sensor. m_x, m_y, and m_z are the torque measured by the force/torque sensor.

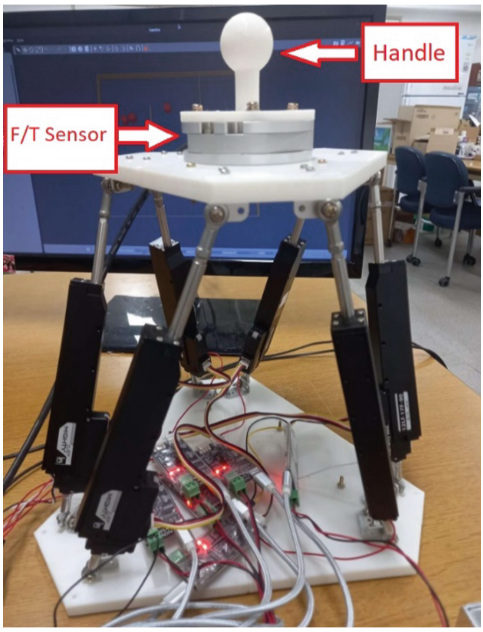

Fig. 1. Haptic device based on Stewart platform

3 Design Inner Position Control

3.1 Dynamic of the Haptic Device

The proposed haptic device is designed by using the admittance model and the inner position control shown in Fig. 2. This research develops the position control method (fault-tolerant control) based on the dynamic model that can ensure the static performance of the haptic device.

The dynamic modeling of the haptic device based on the Stewart Platform can be described as follows:

$$F = M(X)\ddot{X} + V(X, \dot{X}) + G(X) + d = J^T \tau \tag{3}$$

where $X = [t_x, t_y, t_z, \gamma, \beta, \alpha]^T$. F denotes the force vector in the task space. J represents a Jacobian matrix. $\tau \in R^n$ is the force vector in joint space. $V(X, \dot{X})$ is the Coriolis and centrifugal force vector. $G(X)$ is the gravity force vector, and d denotes the unknown disturbance.

The parameters M, V, G in (3) can be divided into nominal and uncertainty elements as follows: $M = M_m + \Delta M$, $V = V_m + \Delta V$, $G = G_m + \Delta G$ where ΔM, ΔV, ΔG are unknown dynamic uncertainties. M_m, V_m, and G_m are the nominal dynamics.

Then, the dynamic Eq. (3) of the Stewart Platform can be expressed as

$$F = M_m\ddot{X} + V_m + G_m + \xi = J^T \tau \tag{4}$$

where $\xi = \Delta M.\ddot{X} + \Delta V + \Delta G + d$.

According to [11], the actuator fault in the system can be modeled as

$$\tau_a = (I - \eta(t))\tau + \varphi(t) \quad (t > t_e) \tag{5}$$

where $\varphi(t) = \left[\varphi_1(t)\ \varphi_2(t)\ ...\ \varphi_n(n)\right]^T$ with $\varphi_1(t)$, $\varphi_2(t)$,..., $\varphi_n(t)$ are bounded functions (bias faults) and $\eta(t) = diag(\eta_1(t), \eta_2(t), ..., \eta_n(t))$ with $\eta_1(t)$, $\eta_2(t)$,..., $\eta_n(t)$ are unknown lost control rate functions (gain faults), $0 \leq \eta_1(t), \eta_2(t), ..., \eta_n(t) \leq 1$. I denotes an identity matrix. τ_a is the torque values at the joints when faults appear and t_e is the time when the faults arise.

Substituting (5) into (4), we get:

$$\ddot{X} = M_m^{-1}\upsilon - M_m^{-1}\left(J^T\eta(t)\tau - J^T\varphi(t) + \xi\right) \tag{6}$$

where $\upsilon = F - V_m - G_m$.

3.2 Extended State Observer-Based Estimation for Faults

To estimate and compensate for the uncertainties, disturbances, and faults, the estimation module based on ESO is described in this subsection.

In the state space, we can express Eq. (6) as:

$$\begin{cases} \dot{\psi}_1 = \psi_2 \\ \dot{\psi}_2 = M_m^{-1}\upsilon + \psi_3 \end{cases} \tag{7}$$

where $\psi_1 = X \in R^n$, $\psi_2 = \dot{X} \in R^n$, $\psi_3 = -M_m^{-1}\left(J^T\eta(t)\tau - J^T\varphi(t) + \xi\right)$. ψ_3 denotes the extended state of the system.

The standard ESO has several drawbacks such as the peaking phenomenon and sensitivity to high-frequency measurement noise. Therefore, to reduce the effect of these drawbacks on the system, a new extended state observer proposed in [9] for the system (7) can be designed as:

$$\begin{cases} \dot{\theta}_1 = \frac{\rho_1}{\sigma}(\psi_1 - \theta_1)\,,\ \widehat{\psi}_2 = \frac{\rho_1}{\sigma}(\psi_1 - \theta_1) \\ \dot{\theta}_2 = M_m^{-1}\upsilon + \frac{\rho_2}{\sigma}\left(\widehat{\psi}_2 - \theta_2\right),\ \widehat{\psi}_3 = \frac{\rho_2}{\sigma}\left(\widehat{\psi}_2 - \theta_2\right) \end{cases} \tag{8}$$

where $\theta_1, \theta_2 \in R^n$, $0 < \sigma < 1$ is a small positive constant. ρ_1, ρ_2 are positive constants. $\widehat{\psi}_1, \widehat{\psi}_2, \widehat{\psi}_3$ are observer states.

The convergence of the ESO (8) was shown in [9]. For the system (7) and the ESO (8), there exists $\varepsilon > 0$ and $T > 0$ so that $\left|\psi_i(t) - \widehat{\psi}_i(t)\right| \leq \varepsilon,\ \ 2 \leq i \leq 3,\ \forall t \geq T$.

3.3 Inner Position Control for the Haptic Device

The fault-tolerant control based on Nonsingular Fast Terminal sliding mode control is designed for a Stewart Platform in this part. We select the sliding mode manifold of NFTSMC as

$$s = e + \mu_1 e^{p_1/p_2} + \mu_2 \dot{e}^{r_1/r_2} \tag{9}$$

where r_1, r_2, p_1, and p_2 are positive odd integers, $1 < r_1/r_2 < 2$, $p_1/p_2 > r_1/r_2$ and μ_1, μ_2 are positive constants. The tracking error $e = Xr - X$. X_r is the reference position and orientation of the center of the upper platform. X is the practical position and orientation of the center of the upper platform.

The differential sliding surface (9) is calculated as,

$$\dot{s} = \dot{e} + \mu_1 \frac{r_1}{r_2} |e|^{\frac{p_1}{p_2}-1} \dot{e} + \mu_2 \frac{r_1}{r_2} |\dot{e}|^{\frac{r_1}{r_2}-1} (\ddot{X}_r - \ddot{X}) \tag{10}$$

From (7) and (10), it can be rewritten as,

$$\dot{s} = \dot{e} + \mu_1 \frac{p_1}{p_2} |e|^{\frac{p_1}{p_2}-1} \dot{e} + \mu_2 \frac{r_1}{r_2} |\dot{e}|^{\frac{r_1}{r_2}-1} \left(\ddot{X}_r - M_m^{-1} \upsilon - \psi_3 \right) \tag{11}$$

We can design the AFTC law with an improved reaching law [10] as follows:

$$F = F_e + F_{sw} = J^T \tau \tag{12}$$

in which the equivalent part is

$$F_e = M_m \left(\ddot{X}_r + \frac{1}{\mu_2} \frac{r_2}{r_1} \dot{e}^{2-\frac{r_1}{r_2}} + \frac{\mu_1}{\mu_2} \frac{p_1}{p_2} \frac{r_2}{r_1} |e|^{\frac{p_1}{p_2}-1} \dot{e}^{2-\frac{r_1}{r_2}} - \widehat{\psi}_3 + \omega_2 |s|^h \mathrm{sgn}(s) \right) + V_m + G_m \tag{13}$$

and the switching part is

$$F_{sw} = M_m \omega_1 \tanh\left(\frac{s}{\delta} \right) \tag{14}$$

with $\omega_1 = \frac{2\omega_3}{\lambda + (1-\lambda)\exp(-\zeta(|s|-1))}$, $h = \begin{cases} k \ if \ |s| \geq 1 \\ 1 \ if \ |s| > 1 \end{cases}$, $k, \omega_2, \omega_3, \lambda, \zeta, \delta$ being positive constants, $0 < \lambda < 1, k > 1$.

Theorem: We consider that with the state space form of the Stewart Platform described in (7), a non-singular fast terminal sliding surface presented in (9), the ESO given in (8), and the controller designed in (12), then tracking error will converge to an equilibrium point in a finite time.

Proof:

The Lyapunov function is chosen as $V = \frac{1}{2} s^2 \geq 0$

Then, the differential Lyapunov function V is

$$\dot{V} = s\dot{s} = s \left[\dot{e} + \mu_1 \frac{p_1}{p_2} |e|^{\frac{p_1}{p_2}-1} \dot{e} + \mu_2 \frac{r_1}{r_2} |\dot{e}|^{\frac{r_1}{r_2}-1} \left(\ddot{X}_r - M_m^{-1} (F - V_m - G_m) - \psi_3 \right) \right] \tag{15}$$

Substituting (12) into (15) yields

$$\dot{V} = -\mu_2 \frac{r_1}{r_2} \omega_1 s |\dot{e}|^{\frac{r_1}{r_2}-1} \tanh\left(\frac{s}{\delta} \right) - \mu_2 \omega_2 \frac{r_1}{r_2} |\dot{e}|^{\frac{r_1}{r_2}-1} |s|^{h+1} + \mu_2 \frac{r_1}{r_2} s |\dot{e}|^{\frac{r_1}{r_2}-1} (\widehat{\psi}_3 - \psi_3) \tag{16}$$

$$\dot{V} \leq -\mu_2 \frac{r_1}{r_2} \omega_1 s |\dot{e}|^{\frac{r_1}{r_2}-1} \tanh\left(\frac{s}{\delta}\right) - \mu_2 \frac{r_1}{r_2} |s| |\dot{e}|^{\frac{r_1}{r_2}-1} \left(\omega_2 |s|^h - \varepsilon\right) \leq 0 \tag{17}$$

The system will be stable if the following condition is satisfied:

$$\omega_2 |s|^h \geq \varepsilon \tag{18}$$

When the state system approaches the sliding surface ($|s| < 1$), (18) leads to $|s| \geq \frac{\varepsilon}{\omega_2}$. The value ε can be very small, e.g., 0.001, 0.0001, etc. due to the convergence of ESO (8). We can select a large enough value ω_2, then ε/ω_2 can be near zero. In other words, s will approach the convergence region ε/ω_2 in a finite time, then the tracking error will converge to the equilibrium point within a finite time, and the theorem is proven.

The finite time t_s of the sliding surface that is needed to travel from e(t_r) to e($t_r + t_s$) can be determined in [12] as

$$t_s = \frac{\frac{r_1}{r_2}|e(0)|^{1-r_2/r_2}}{\mu_1\left(\frac{r_1}{r_2}-1\right)} GF\left(\frac{r_2}{r_1}, \frac{\frac{r_1}{r_2}-1}{\left(\frac{p_1}{p_2}-1\right)\frac{r_1}{r_2}}; 1 + \frac{\frac{r_1}{r_2}-1}{\left(\frac{p_1}{p_2}-1\right)\frac{r_1}{r_2}}; -\mu_1 |e(0)|^{p_1/p_2-1}\right) \tag{19}$$

where GF(.) is a Gauss' hypergeometric function.

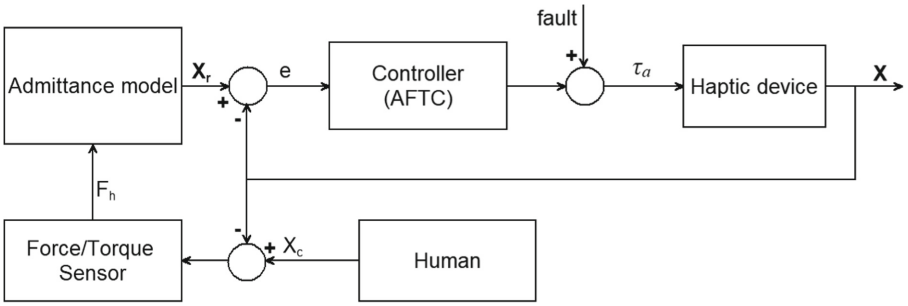

Fig. 2. Admittance control scheme for the haptic device

4 Experiment

4.1 The Performance of the Proposed Controller

This subsection compares the efficiency of NFTSMC without ESO (NFTSMC), NFTSMC with the standard ESO (AFTC-ESO1), and the suggested fault-tolerant method (12) using the ESO (8) (Proposed Controller) for a haptic device based on a Stewart Platform, which was mainly constructed by six MightyZap actuators 12Lf-17F-90 and the moving and fixed platforms shown in Fig. 1. A six-axis force/torque sensor RFT80-6A01 is mounted on the moving platform and the handle is installed on the sensor.

The NFTSMC without the ESO can be expressed as:

$$F = M_m\left(\ddot{X}_r + \frac{1}{\mu_2}\frac{r_2}{r_1}\dot{e}^{2-\frac{r_1}{r_2}} + \frac{\mu_1}{\mu_2}\frac{p_1}{p_2}\frac{r_2}{r_1}e^{\frac{p_1}{p_2}-1}\dot{e}^{2-\frac{r_1}{r_2}} + \omega_1 sign(s) + \omega_2 s\right) + V_m + G_m \tag{20}$$

On the other hand, the standard ESO for the system (7) can be given as:

$$\begin{cases} \dot{\widehat{\psi}}_1 = \widehat{\psi}_2 + \frac{\rho_1}{\sigma}\left(\psi_1 - \widehat{\psi}_1\right) \\ \dot{\widehat{\psi}}_2 = M_m^{-1}\upsilon + \frac{\rho_2}{\sigma^2}\left(\psi_1 - \widehat{\psi}_1\right) + \widehat{\psi}_3 \\ \dot{\widehat{\psi}}_3 = \frac{\rho_3}{\sigma^3}\left(\psi_1 - \widehat{\psi}_1\right) \end{cases} \tag{21}$$

where $\widehat{\psi}_1, \widehat{\psi}_2, \widehat{\psi}_3$ are observer states. $\sigma < 1$ is a small positive constant. ρ_1, ρ_2, ρ_3 are positive constants selected such that the following polynomial is Hurwitz: $s^3 + \rho_1 s^2 + \rho_2 s + \rho_3$. Then, the AFTC-ESO1 controller is designed similarly to (12), but $\widehat{\psi}_3$ in the controller is an observer state of (21).

To test the robustness of the proposed controller compared with the other controllers, it was assumed that faults occur at leg 2, leg 4, and leg 6 from the tenth second. The torque functions of actuators with the existence of faults were defined in (5) where the gain faults can be assumed as $\eta_1(t) = 0$, $\eta_2(t) = 0.2 + 0.3\sin(\pi t)$, $\eta_3(t) = 0$, $\eta_4(t) = 0.3 + 0.1\cos(3t + 2)$, $\eta_5(t) = 0$, $\eta_6(t) = 0.25 + 0.2\cos(t + 7)$ and the bias faults can be assumed as $\varphi_1(t) = 0$, $\varphi_2(t) = 0.3\cos(0.5t + 10)$, $\varphi_3(t) = 0$, $\varphi_4(t) = 0.2\sin(3t)$, $\varphi_5(t) = 0$, and $\varphi_6(t) = \sin(t + 5)$. For the ESO (8), the parameters are set as $\rho_1 = 1$, $\rho_2 = 1$, and $\sigma = 0.09$. The parameters of the standard ESO (21) are given as $\rho_1 = 3$, $\rho_2 = 3$, $\rho_3 = 1$, and $\sigma = 0.09$. The parameters in AFTC law (12) and (20) are selected as $\mu_1 = 0.1$, $\mu_2 = 0.02$, $\mathrm{p}_1 = 27$, $\mathrm{p}_2 = 19$, $\mathrm{r}_1 = 21$, $\mathrm{r}_2 = 19$, $\omega_3 = 0.1$, $\omega_2 = 400$, $\lambda = 0.1$, $\zeta = 0.2$, $\delta = 0.1$, $\mathrm{k} = 1.1$. The random movements of the upper platform were given by the force impacting on the handle through the admittance model (2) where $M_i = 1$, $B_i = 70$, $K_i = 800$.

For teleoperation of a mobile robot, just two degrees of freedom (DOF) of Stewart platform are used. Thus, we considered the performance of x and y directions only, and neglected the remaining DOFs in this study. In addition to observing the result figures, the mean absolute error (MAE) (22) of each controller was also used for the performance evaluation.

$$MAE = \frac{1}{m}\sum_{m=1}^{m}|X_{ri} - X_i| = \frac{1}{m}\sum_{i=1}^{m}|e_i| \tag{22}$$

where X_{ri} is the reference trajectory, X_i is the practical trajectory, m is the sample size. $e_i = X_{ri} - X_i$.

Figure 3 and Table 1 show experimental results of the haptic device using NFTSMC, AFTC-ESO1, and Proposed Controller for x and y directions. It can be seen that the performance of AFTC-ESO1 and Proposed Controller were better than NFTSMC in

the first ten seconds due to the estimation and compensation of the standard ESO (8) and ESO (21) in the control laws for unknown uncertainties and disturbances of the system. Next, after ten seconds, the actuator faults occurred and the controllers showed significantly different performances. Thanks to the compensation of the ESO (8) and ESO (21), AFTC-ESO1 and Proposed Controller presented superior performance compared to NFTSMC for control tasks even though the faults arose. The proposed Controller using the ESO (8) was a bit more effective than AFTC-ESO1. Besides, the handle of the haptic device using NFTSMC does not move smoothly under the presence of faults, which causes uncomfortable state for the operator. In summary, the haptic device using the Proposed Controller has high precision and moves smoothly compared with the other controllers.

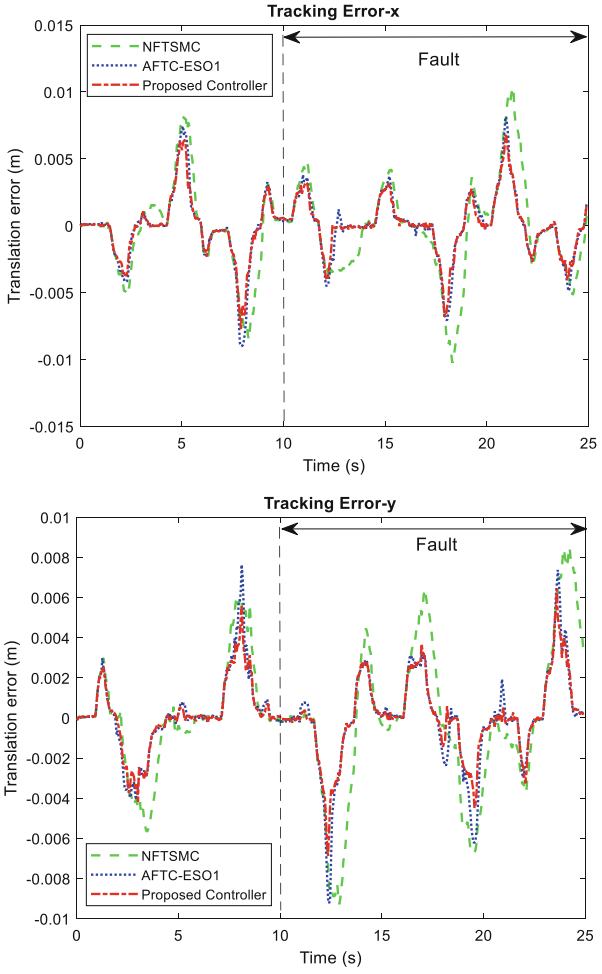

Fig. 3. The performance of the haptic device using NTSMC, AFTC-ESO1, and proposed controller

Table 1. The mean absolute errors for x and y directions

	NFTSMC	AFTC-ESO1	Proposed controller
MAE-x	0.0026	0.0016	0.0015
MAE-y	0.0024	0.0014	0.0012

4.2 Teleoperation of a Mobile Robot in the Virtual Environment

Figure 4 shows the teleoperation scheme of a mobile robot. The proposed haptic device with the faulty assumption in subsect. 4.1 was tested for teleoperation of the slave robot in the virtual environment built in Gazebo and shown in Fig. 5. The virtual environment includes a mobile robot and obstacles. The mobile robot is equipped with a Lidar sensor to detect obstacles. The laser scanner provides an angular solution of 1°, an angular range of 360°, and a distance range of approximately 3.5 m at a scan rate of approximately 300 rpm. The obstacles were different shapes and sizes, and were comprised of cylinders, cubes, and walls. The haptic device was connected to the computer and communicated with the mobile robot via ROS (Robot Operating System) software platform. According to [4], a logical position of the haptic handle can be mapped to the motion parameters of the mobile robot. For this research, the position command x and y were mapped to the speed rate and turning rate, respectively shown in Fig. 6. In this experiment, the operator remotely controls the mobile robot by moving the handle of the haptic device. The mission is that the operator controls the mobile robot to move from the start point to the goal point as fast as possible while simultaneously avoiding the obstacles on the given route shown in Fig. 5.

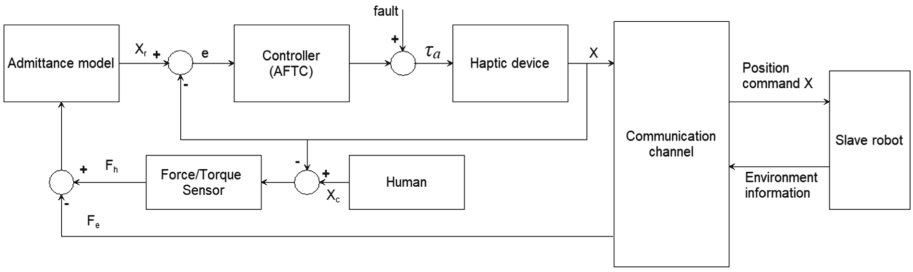

Fig. 4. Teleoperation scheme of a mobile robot

The position of the haptic handle and contact force on the handle measured by the force/torque sensor are shown in Fig. 7. Due to the measurement noise and the sensitivity of the F/T sensor, there were contact force oscillations lower than 5N in Fig. 7b, but it did not cause difficulty in controlling the haptic handle. It took approximately 145 s to complete the mission and the robot approached the obstacles two times. When the robot closed to obstacles two and four, the force feedback was provided to the haptic

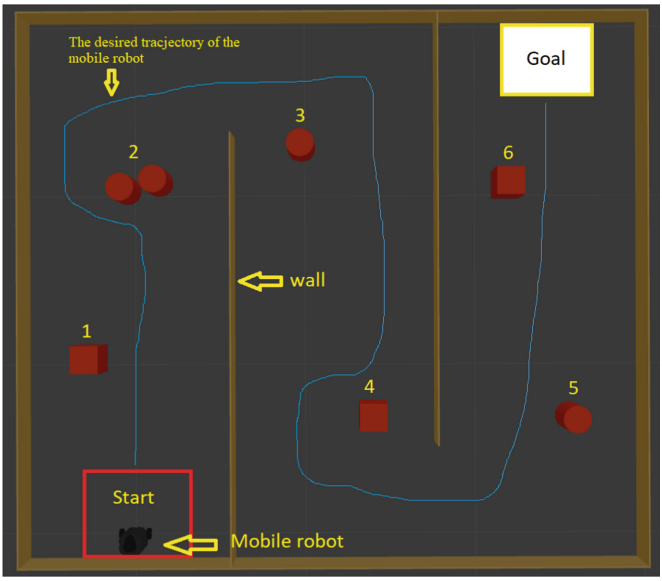

Fig. 5. A mobile robot in a virtual environment

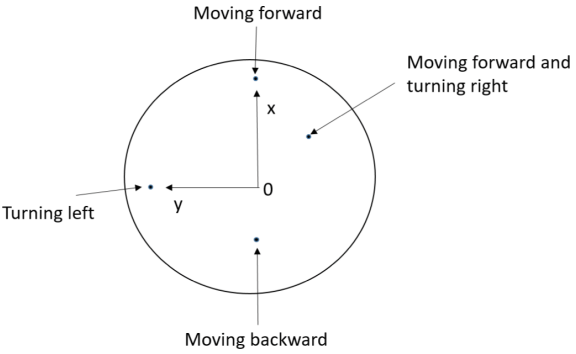

Fig. 6. Mapping a logical point (x, y) to motion parameters (speed rate, turning rate)

device to drive the handle backward at the 16^{th} and 83^{rd} seconds, which made the contact force increase and the robot move away from the obstacles. In the real field, this would protect the robot from damage due to an unexpected collision. These results illustrated the adequacy and effectiveness of the proposed haptic device for the teleoperation of a mobile robot.

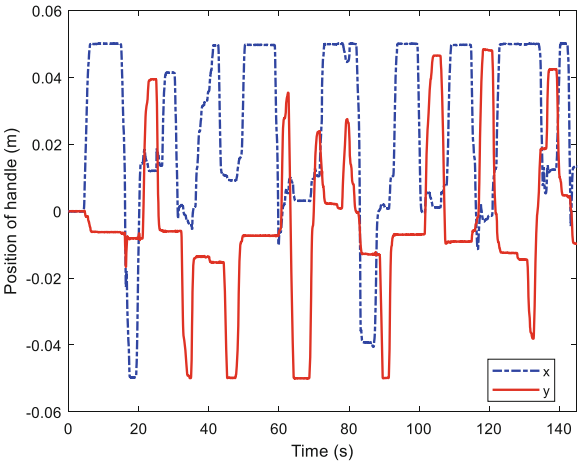

a)

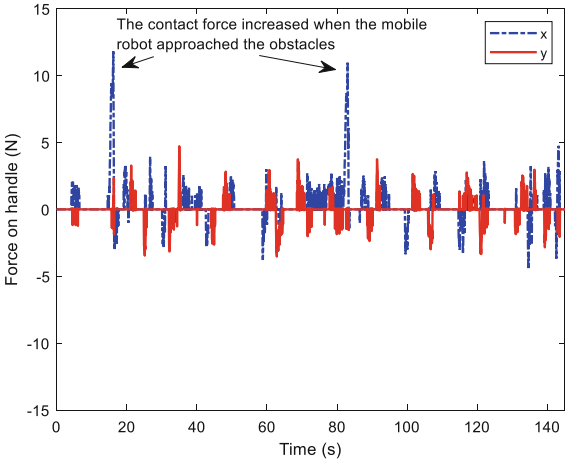

b)

Fig. 7. Experimental results of teleoperation. a) Movement of the haptic handle to control a mobile robot. b) Contact force on the haptic handle

5 Conclusion

In this paper, the development of a haptic device based on a Stewart platform using the admittance model and fault-tolerant control was presented. The admittance model was used to convert force input to the handle position. The position control based on a fault-tolerant algorithm was developed to track the desired position given by the admittance model. To prove the effectiveness of the proposed fault-tolerant controller compared to the other controllers, the same desired trajectory and fault functions were applied for all controllers. The tracking performance in the experiment showed good performance of the Proposed Controller compared with the NFTSMC and AFTC-ESO1. Furthermore,

the Proposed Controller illustrated the robustness trait and improved accuracy even though unknown disturbances and faults appeared in the system. The handle of the haptic device using Proposed Controller moved smoother than using the other controller, which makes the operator comfortable for controlling the haptic device. Finally, teleoperation of a mobile robot in a virtual environment was implemented to assess the proposed haptic device. The results demonstrated that the proposed master device was effective for teleoperation of the mobile robot.

In the future, the teleoperation of an actual mobile robot via wireless communication will be investigated. Furthermore, the proposed haptic device will be applied for teleoperation of the 6-DOF model like an unmanned aerial vehicle (UAV).

References

1. Abdossalami, A., Sirouspour, S.: Adaptive control for improved transparency in haptic simulations. IEEE Trans. Haptics. **2**, 2–14 (2009). https://doi.org/10.1109/TOH.2008.18
2. Park, H., Lee, J.M.: Adaptive impedance control of a haptic interface. Mechatronics **14**, 237–253 (2004). https://doi.org/10.1016/S0957-4158(03)00040-0
3. Na, U.J.: A new impedance force control of a haptic teleoperation system for improved transparency. J. Mech. Sci. Technol. **31**, 6005–6017 (2017). https://doi.org/10.1007/s12206-017-1145-6
4. Ju, C., Son, H.: Il: Evaluation of haptic feedback in the performance of a teleoperated unmanned ground vehicle in an obstacle avoidance scenario. Int. J. Control. Autom. Syst. **17**, 168–180 (2019). https://doi.org/10.1007/s12555-017-0721-y
5. Van, M., Ge, S.S., Ren, H.: Finite time fault tolerant control for robot manipulators using time delay estimation and continuous nonsingular fast terminal sliding mode control. IEEE Trans. Cybern. **47**, 1681–1693 (2017). https://doi.org/10.1109/TCYB.2016.2555307.
6. Zhang, H., Han, J., Luo, C., Wang, Y.: Fault-tolerant control of a nonlinear system based on generalized fuzzy hyperbolic model and adaptive disturbance observer. IEEE Trans. Syst. Man Cybern. Syst. **47**, 2289–2300 (2017). https://doi.org/10.1109/TSMC.2017.2652499.
7. Le, Q.D., Kang, H.J.: Implementation of fault-tolerant control for a robot manipulator based on synchronous sliding mode control. Appl. Sci. **10**, 1–19 (2020). https://doi.org/10.3390/app10072534
8. Yin, S., Luo, H., Ding, S.X.: Real-time implementation of fault-tolerant control systems with performance optimization. IEEE Trans. Ind. Electron. **61**, 2402–2411 (2014). https://doi.org/10.1109/TIE.2013.2273477
9. Ran, M., Li, J., Xie, L.: A new extended state observer for uncertain nonlinear systems. Automatica **131**, 109772 (2021). https://doi.org/10.1016/j.automatica.2021.109772
10. Le, D.-V., Ha, C.: Finite-time fault-tolerant control for a Stewart platform using sliding mode control with improved reaching law. IEEE Access **10**, 43284–43302 (2022). https://doi.org/10.1109/access.2022.3165091
11. Guo, J., Qi, J., Wu, C.: Robust fault diagnosis and fault-tolerant control for nonlinear quad rotor unmanned aerial vehicle system with unknown actuator faults. Int. J. Adv. Robot. Syst. **18**, 1–14 (2021). https://doi.org/10.1177/17298814211002734
12. Yang, L., Yang, J.: Nonsingular fast terminal sliding-mode control for nonlinear dynamical systems. Int. J. Robust Nonlinear Control **23** (2015). https://doi.org/10.1002/rnc.1666